Fatigue design of A356T6 under multiaxial loading

Y. NADOT[1], M. ROY[2], D.M. MAIJER[2], M. IBEN HOURIA[3], R. FATHALLAH[3] [a]

1 Institut PPRIME - CNRS - Université de Poitiers - ENSMA - UPR 3346 – Département Mécanique des Matériaux - Téléport 2 - 1 Avenue Clément Ader - BP 4019 – 86961 FUTUROSCOPE CHASSENEUIL Cedex– France

2 Dept. of Materials Engineering, The University of British Columbia, Vancouver, BC, Canada V6T 1Z4

3 LGM, Ecole nationale d'Ingénieurs de Sousse, Avenue 18 janvier 1952 4000 Sousse, Tunisia

Abstract Experimental Kitagawa diagrams are produced for cast A356 T6 containing natural and artificial defects. Results are obtained for three different loadings: tension, torsion and combined tension-torsion, for a load ratio R = -1. The experimental critical defect size determined is 400 +/- 100 μm in A356 T6 under multiaxial loading. Below this value, the microstructure governs the fatigue limit mainly through the SDAS. We compared four theoretical approaches to simulate Kitagawa diagram: Murakami's equation, a defect is equivalent to a crack using Linear Elastic Fracture Mechanics, the Critical Distance Method (CDM) proposed by Susmel and Taylor and the gradient approach proposed by Nadot. It is shown that CDM and gradient methods give good results but need three fatigue data for the identification.

1 MATERIAL AND EXPERIMENTAL RESULTS

The material employed in this study was Low-Pressure Die Cast (LPDC) strontium modified A356 (Al-7Si-0.3Mg). Tensile testing has resulted in a modulus of elasticity of 66 GPa, Poisson's ratio of 0.3, a yield strength of 164 MPa and an ultimate tensile strength of 317 MPa. While all specimens came from castings made with permanent steel dies, the majority of specimens came from a wedge-shaped casting, and a lesser number were cut directly from an automotive wheel. The wheel casting was actively cooled during solidification while the wedge casting was passively left to cool. As these two casting types provided a wide range of solidification conditions, so too did the specimens from a defect and microstructure standpoint. Therefore, the fatigue behaviour characterized in the current work is directly applicable to commercial castings.
Experimental Kitagawa diagrams are reported here for the three different loadings as well as the most representative SEM fracture surface features. Pure tension results are reported on Figure 1 and SEM observations on Figure 2, tension-torsion combined tests with $\sigma = \tau$ on Figures 3 and 4 and finally pure torsion results on Figures 5 and 6. All Kitagawa diagrams are presented with the same scale in a bi-linear diagram presentation style. The fracture surfaces are observed first by eyes in order to get the macroscopic features of the crack path. Then comes SEM observations in order to show some details of the initiation area and, when possible, the defect size measurement. The defect size parameter used is the 'area' parameter proposed by Murakami [1]. Cast A356 T6 contains different types of defects also reported by [2-4]. Defects can be gas pores, shrinkages, oxides films or inter-metallic inclusions.

Figure 1 presents the experimental Kitagawa diagram under pure tension and R = -1. In all samples, the initial defect size was easy to determine and the fracture plane was always perpendicular to the direction of the maximum principal stress. The first remarkable point from this curve is the relative high critical defect size: the tests T6, A1 and A2 have a very low impact on the fatigue limit (8 % reduction). The material is sensitive to defect when the size is bigger than 500 μm under tension. It is interesting to point out that this does not depend on the type of defect.

Figure 2 shows fracture surfaces for M3, T6 and A1. In the first case (M3) a very small subsurface defect is at the origin of the crack. This defect seems to be an oxide-related pore but the size remains very small here. T6 sample failed from 400 μm shrinkage at the surface of the sample. A1 failed from the 400 μm induced artificial defect. Both T6 and A1 give the same fatigue limit so that we can conclude that the area parameter is able to correlate different types of defects. Nevertheless, this conclusion should be done also for bigger defects with higher impact on the fatigue limit. Fracture surfaces for A3 and A4 are very similar to A2 with the artificial defect at the initiation point.

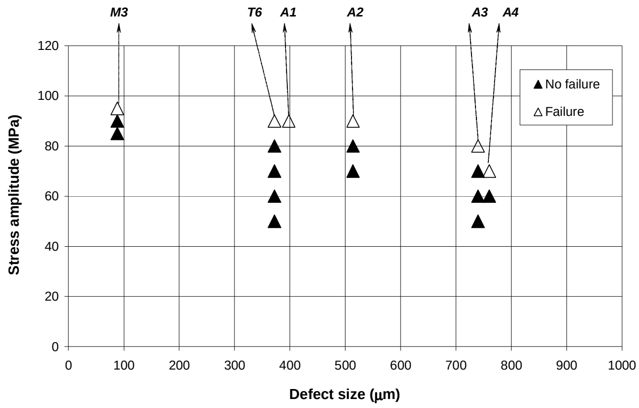

Figure 1: Kitagawa type diagram for A356-T6 under tension, R = -1.

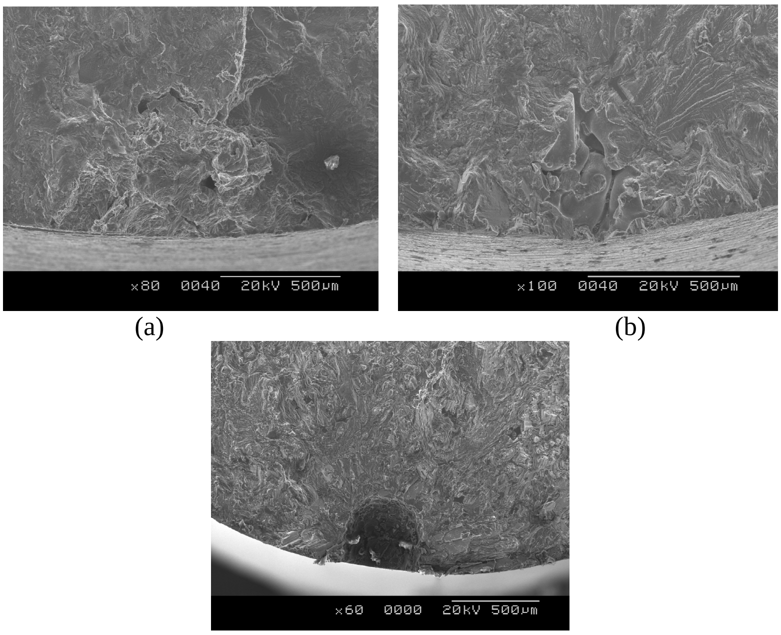

(a) (b)

(c)

Figure 2: SEM observation of initiation site defect (tension, R = -1) (a) M3 (b) T6 (c) A1

Figure 3 presents the experimental Kitagawa diagram under pure torsion and R = -1. The experimental points presented on the curve below 100 µm are classified as either 'no defect' or 'not identified defect'. The samples have been separated with different defect size between 0 and 100 µm but it is only in order to make the graph clear, it is not related to the defect size because there is no. The first remarkable conclusion on the Kitagawa diagram under torsion is the scatter. The fatigue limits vary from 55 to 95 MPa for samples with 'no defect' or 'not identified defect'. This represents a huge scatter compared to the other results obtained for the other load cases.

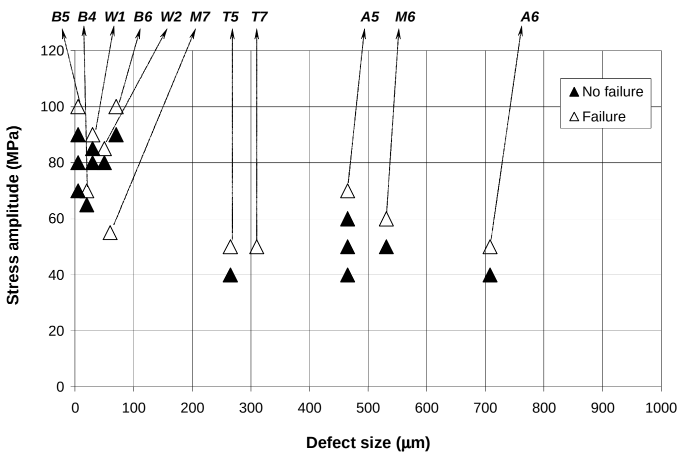

Figure 3: Kitagawa type diagram for A356-T6 under torsion, R = -1.

The general feature of the fracture surface under pure torsion is very tortuous as show on Figure 4a. Many shear cracks in the two maximum shear planes are activated so that the final fracture surface reveals many different initiation sites. That is not the case for the other loadings. Even with careful examination of the fracture surface at each suspected initiation point, like in Figure 4b, it is not always possible to determine a defect as defined in the introduction of this section. The multiple initiation site could be an explanations of the scatter observed. It could be also the fact that we were not able to find the critical defect on the complex fracture surface. In order to analyze this point into more details, samples B4, M7, T5 and T7 have been cut and polished in order to observe the material just below the fracture surface. We were not able to find any defect close to the fracture surface, there is no evidence of higher porosity amount or any oxide film. The critical defect size under pure torsion is close to 300 µm, which is smaller than under tension. This critical defect size should be clarified by other tests on samples containing 300 µm artificial defects.

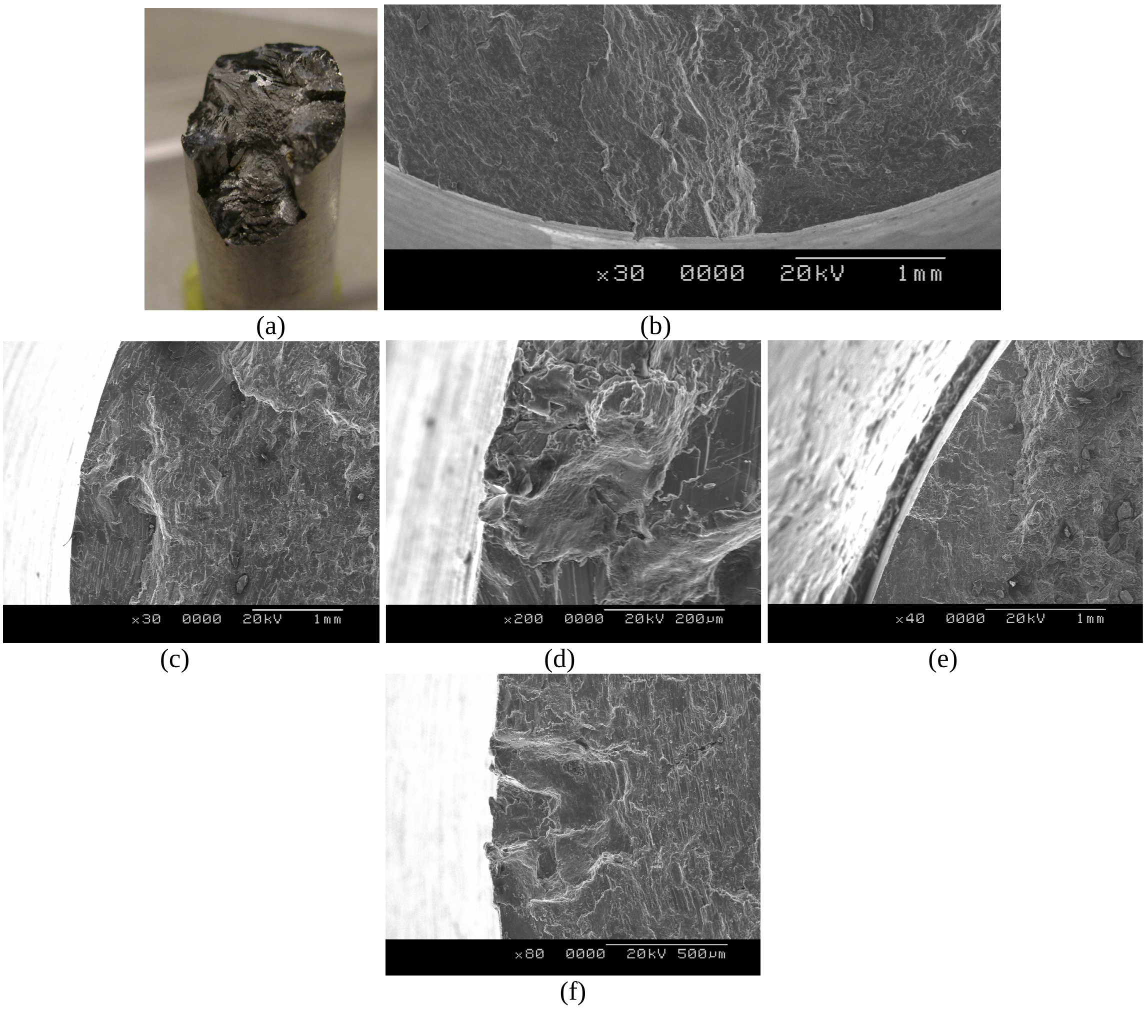

Figure 4: SEM observation of initiation site defect (torsion, R = -1) (a-b) W2 (c-d-e) T7 (f) M6

Figures 4c, 4d and 4e present another example of the difficulties we had to determine the defect size under pure torsion. Figure 4a shows the suspected initiation area. Figure 4b details the defect that is supposed to be at the origin of the crack. This defect looks like an oxide film but this is really difficult to separate from the oxide built up produced by crack lips contact during shear crack propagation. In many different locations around the fracture surface we can observe these black oxides produces during the shear crack propagation. Therefore we can not be really sure that this is a 300 µm defect size. T7 sample contains also an artificial defect (230 µm) that we were able to see on Figure 4e because this defect was kind enough to be on the fracture plane of the major crack from the oxide defect. Figure 4e reveals the secondary crack initiated from the artificial defect. Nevertheless, this defect was less harmful that the oxide film. Finally Figure 4f presents another oxide film at the origin of the failure. It is to be noticed that when comparing with the area parameter, oxide film and artificial defect seems to behave similarly.

Figure 5 presents the experimental Kitagawa diagram under combined tension-torsion and R = -1. In this curve, no artificial defects are involved, only natural ones. Macroscopic fractures surfaces are similar to tension ones:

flat surface in the plane perpendicular to the direction of the maximum principal stress with a clear identification of the initiation area. The Kitagawa curve shows a very small influence of 500 µm defect. In fact for defects below this size, it seems that there is no influence of the defect on the fatigue limit.

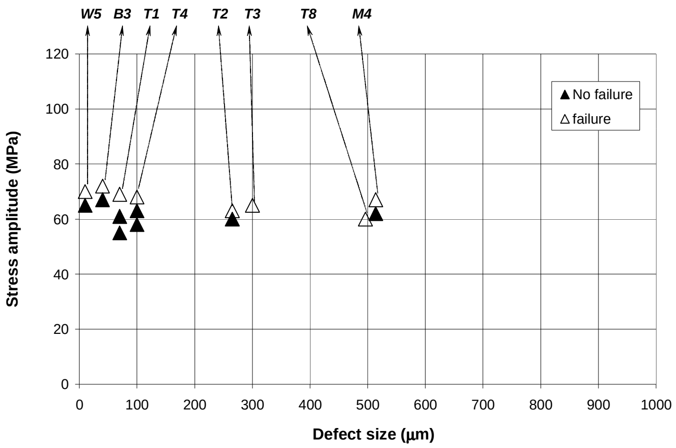

Figure 5: Kitagawa type diagram for A356-T6 under tension-torsion, R = -1.

Figure 6a on sample B3 gives an illustration of the initiation area when there is no defect at the origin of the failure. Figure 6b on sample M4 shows a big sub surface pore with a size of 500 µm. Finally, Figure 6c reveals the shrinkage at the origin of the failure on sample T8. It is interesting to point out that M4, which is a big defect but not at the surface, leads to the same fatigue limit that T8.

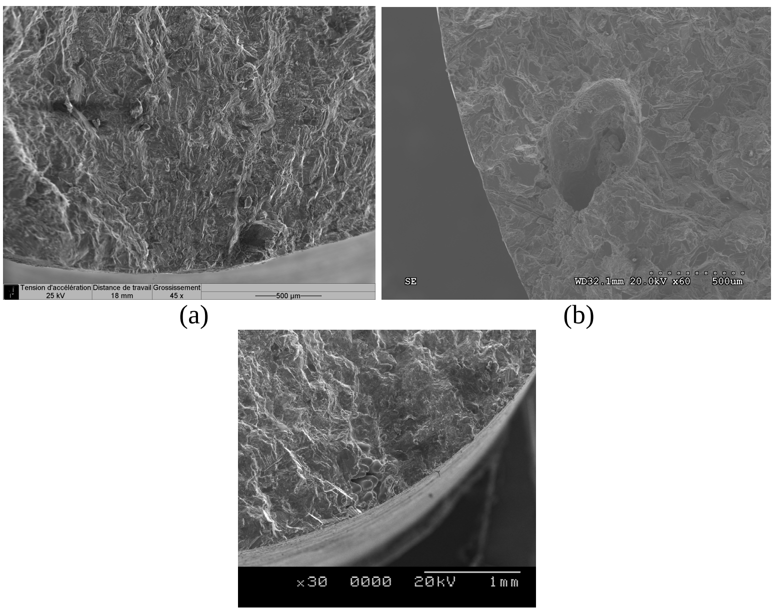

(a) (b)

(c)

Figure 6: SEM observation of initiation site defect (tension-torsion, R = -1) (a) B3 (b) M4 (c) T8

From the previous fatigue results obtained on A356 T6 containing artificial and natural defects, we can conclude that the critical defect size that does not affect the fatigue limit is relatively large. It ranges from 300 to 500 µm depending on the loading type. It is also interesting to observe that when the defect is described by the 'area' parameter, an artificial defect behaves similarly to a shrinkage or an oxide film against fatigue limit. It is another demonstration that this parameter is really powerful to describe the morphology of a given defect. From the pure torsion results, it is not so easy to find the initial defect size due to the complex topology of the fracture surface and the multiple initiation sites. This last point should be studied into more details especially because we were not able to find any fatigue results under torsion on A356 T6 with experimental characterization of defect size in the literature.

2 COMPARISON OF MULTIAXIAL FATIGUE CRITERIA

LEFM describes crack propagation threshold with the amplitude of the stress intensity factor ΔK, a function of crack length a_c and stress amplitude $\Delta\sigma_c$. The defect size is given trough the 'area' parameter that is transformed into a semi circular crack here. The relation between the fatigue limit and the defect size is given by:

$$\Delta\sigma_C = \frac{\Delta K_{th,eff}}{Y\sqrt{\sqrt{2\pi}\sqrt{area}}}$$

Where Y is the crack shape factor and $\Delta K_{th,eff}$ is the effective stress intensity factor threshold.

With a spherical defect: $Y = \frac{2}{\pi}$. $\Delta K_{th,eff} = 1.5 MPa\sqrt{m}$ for A356-T6 alloy; this value was not experimentally determined in our material but from a large compilation of published data from [5-10].

Murakami proposes to represent the defect as a surface entity and introduces the $\sqrt{area}$ parameter to describe defect size. He justifies this choice using fracture mechanics concepts. Observing non-propagating cracks in a small stressed zone around de defect, he considers that endurance threshold corresponds to crack growth threshold. He shows that the maximum stress intensity factor $K_{I\,max}$ is linearly related to the $\sqrt{area}$ parameter for different crack geometry and then links the endurance threshold and this size parameter. He shows that for a given Vickers hardness, fatigue crack growth threshold depends mainly on $\sqrt{area}$ parameter. Murakami has proposed an empirical equation based on the defect size ($\sqrt{area}$) and the material hardness to predict the fatigue limit of materials containing small defects.

Murakami proposed the following empirical relations for tension loading:

$$\sigma_W = \frac{A(H_v + 120)}{\left(\sqrt{area}\right)^{1/6}}\left[\frac{1-R}{2}\right]^{\alpha}$$

With $A = 1.43$ for surface defects and $A = 1.56$ for internal defects and $\alpha = 0.226 + H_v * 10^{-4}$.

For torsion loading and surface defects, the fatigue limit is given by the following equation:

$$\tau_W = \frac{0.93(H_v + 120)}{F(b/a)\left(\sqrt{area}\right)^{1/6}}\left[\frac{1-R}{2}\right]^{\alpha}$$

With $F(b/a) = 0.0957 + 2.11(b/a) - 2.26(b/a)^2 + 1.09(b/a)^3 - 0.196(b/a)^4$ and $b/a = 1$ for spherical defects.

For combined tension-torsion loading, the fatigue limit is given by the following relation:

$$\sigma_1 + k\sigma_2 = \frac{A(H_v + 120)}{\left(\sqrt{area}\right)^{1/6}}\left[\frac{1-R}{2}\right]^{\alpha}$$

Where σ_1 is the maximum principal stress, σ_2 is the minimum principal stress and $k = -0.18$ for cracks emanating from a round defect.

There are two parameters that have to be identified for Murakami's relations: the macroscopic Vickers hardness (H_v = 80 MPa for A356 T6) and the b/a parameter (b/a = 1 for spherical defect). Murakami's equation is very simple to identify but the limitation is mainly due to the description of the stress state that is not able to take into account for a general multiaxial loading.

The 'critical distance' approach and the 'gradient' one needs a multiaxial fatigue criterion to be applied. In this paper, we decided to use the equivalent stress proposed recently by Vu [11] that aims to describe the multiaxial behavior for complex loading using invariant approach. This equivalent stress needs only analytical computations but we could use another criterion so that the following results comparing the approaches are not depending on the criterion.

$$\sigma_{eqVu} = \sqrt{\gamma_1 J'_2(t)^2 + \gamma_2 J^2_{2,mean}(t)^2 + \gamma_3 I_f(I_{1,a}, I_{1,m})} \le \beta$$

With $J'_2(t) = \sqrt{\frac{1}{2}\underline{\underline{S}}_a(t) : \underline{\underline{S}}_a(t)}$ where $\underline{\underline{S}} = \underline{\underline{\Sigma}} - \frac{1}{3}tr(\underline{\underline{\Sigma}})\underline{\underline{I}}$, $J_{2,mean} = \frac{1}{T}\int_0^T J'_2(t)$,

$$I_{1,a} = \frac{1}{2}\left\{\max_{t\in T} I_1(t) - \min_{t\in T} I_1(t)\right\},\quad I_{1,m} = \frac{1}{2}\left\{\max_{t\in T} I_1(t) + \min_{t\in T} I_1(t)\right\} \text{ and } I_f(I_{1,a}, I_{1,m}) = I_{1,a} + \alpha I_{1,m}$$

The values of $\gamma_1, \gamma_2, \gamma_3$, β and α depend on the strength of the metal and are identified using the parameters t_{-1}, f_{-1} and R_m. For the A356 T6 alloy, $\gamma_3 = \frac{t_{-1}^2 - \frac{f_{-1}^2}{3}}{f_{-1}} = 41.1MPa$, $\beta = t_{-1} = 80MPa$ and $R_m = 317MPa$ so $\gamma_1 = 0.65$, $\gamma_2 = 0.8636$ and $\alpha = 1$.

The second input data needed by both 'critical distance' and 'gradient' approaches is the stress distribution around the defect. In order to compute local stresses around the defect represented here by a spherical void, the analytical theory of Eshelby have been used.

This CDM is based on the approach proposed by Susmel and Taylor. [12] This approach describes the influence of the defect through the measurement of the stresses to compute the equivalent fatigue stress at a given distance from the defect. We need therefore the evaluation of the stress field around the defect as explained before. The maximum equivalent stress is calculated at the critical distance L/2 from the tip of the notch. The fatigue limit σ_C is established as follow:

$$\underset{\sigma=\sigma_C}{Max}\left(\sigma_{eqVu}\left(\frac{L}{2} \right) \right) = \beta$$

With σ the nominal applied stress.

The parameter we have to identify to use this criterion is the parameter L/2. This distance is the distance from the notch tip to the point where $\sigma_{eqVu} = \beta$. We need therefore an experimental fatigue limit for a given defect size to make the identification of L/2. The following case has been used $\sigma_{\infty ref} = 85MPa$ for $\sqrt{area}_{ref} = 400\mu m$. It has been found that L/2 = 79µm.

Nadot, Gadouini [13, 14] proposed to compute an equivalent stress that includes the effect of the defect through the description of the stress gradient around the defect. The criterion is written as follow:

$$\sigma_{eq}^{*} = \sigma_{eqVu,Max}\left[1 - b_g \frac{\nabla \sigma_{eqVu}}{\sigma_{eqVu,Max}} \right] \le \beta$$

Where $\nabla \sigma_{eqVu} = \frac{\sigma_{eqVu,Max} - \sigma_{eqVu,\infty}}{\sqrt{area}}$ is the equivalent stress gradient,

$\sigma_{eqVu,Max}$ is the maximum equivalent stress calculated at the tip of the defect and

$\sigma_{eqVu,\infty x}$ is the nominal equivalent stress calculated far from the defect.

To use this criterion, the parameter b_g has to be identified. It has the dimension of a length ($\sqrt{area}$). This parameter allows accounting for the defect geometry and is calculated using fatigue limit of material containing a known artificial defect. Identification is performed on the reference loading case ($\sigma_{\infty ref} = 85MPa$ and $\sqrt{area}_{ref} = 400\mu m$):

$$b_g = \sqrt{area}_{ref} \left(\frac{\sigma_{eqVu,Max} - \sigma_{eqVu,\infty}}{\sigma_{eqVu,Max} - \beta} \right)$$

The calculation of the stress field around the defect is performed using the analytical computation explained before.

Under tension, critical distance and gradient approaches are very good for the values but this is not surprising because one experimental point is used for the identification. The trend is also well described. Murakami's equation leads to non conservative result but the trend is well described. LEFM gives conservative results with a good trend. Under torsion, all approaches are relatively good for values and trend; expect Murakami that is again non conservative and critical distance that tend to assess a small allowable defect size. Under combined loading, all approaches are non conservative except Murakami. Again the critical defect size is largely underestimated by the critical distance theory.

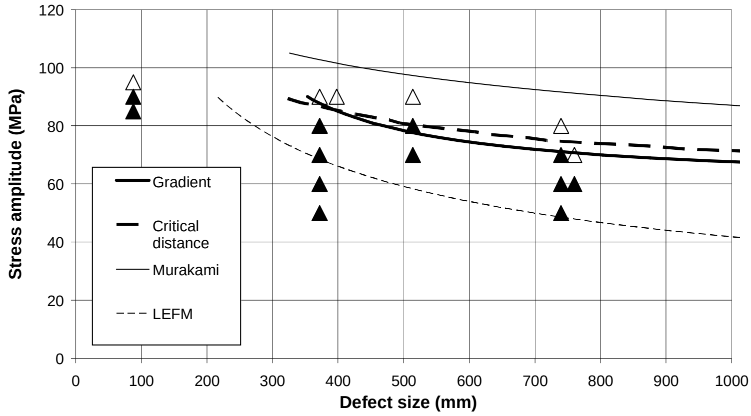

Figure 7: comparison between experimental results and simulations (tension, R -1).

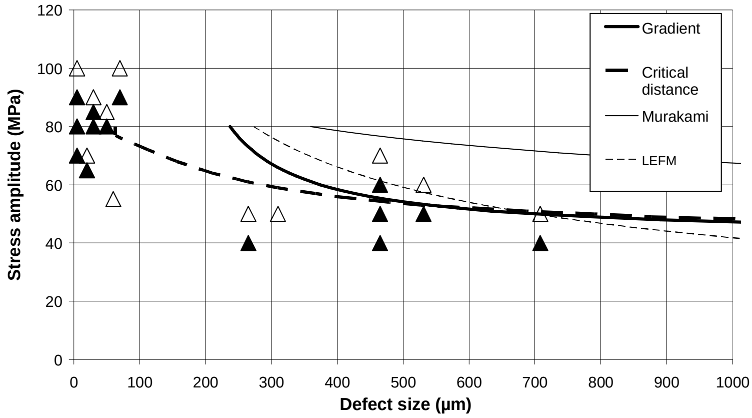

Figure 8: comparison between experimental results and simulations (torsion, R -1).

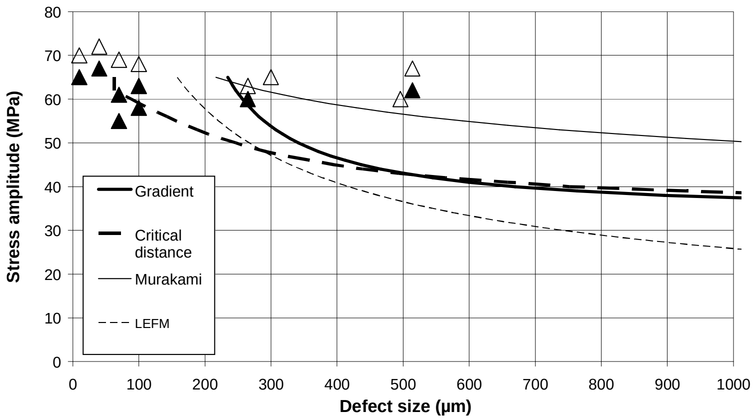

Figure 9: comparison between experimental results and simulations (tension-torsion, R -1).

Figure 10 gives another viewpoint on this comparison by plotting the error between simulation and each experimental result for the four approaches and all load cases. Negative values are related to non conservative assessment and positive to conservative ones. We can also average the absolute error given by each approach; this leads to the following result LEFM = 19 %, Murakami = 20 %, critical distance = 11 % and gradient = 9 %. From this general average comparison we can conclude that the description of the defect through the elastic stress field (gradient or critical distance approach), gives better results that LEFM or Murakami. But if we include in the comparison the 'identification cost', then Murakami's equation remains very good because you can give the fatigue limit of the material for different defect sizes, three load cases using only the macroscopic hardness of the material. LEFM gives also in average interesting results related to the fact that only one experimental parameter is used: the effective threshold stress intensity factor for long cracks. Both critical distance method proposed by Susmel and Taylor and gradient one proposed by Nadot are good in average but you have to describe the elastic stress field around the inclusion and get three experimental fatigue limits including one with a defect. It is important to note that elastic computation of stresses is relevant in the case of A356-T6 because fatigue limit is half the yield stress so that there is a very little amount of plasticity at the tip of the defect.

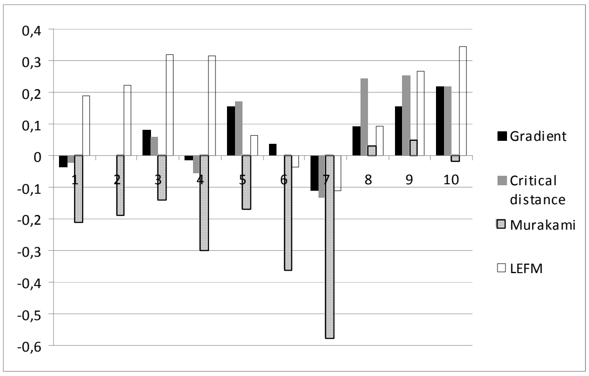

Figure 10: Quantitative comparison between simulations and experimental results for the four approaches tested.

3. CONCLUSIONS

- In cast A356-T6 submitted to multiaxial fatigue loading, fatigue cracks can initiate either on casting defects or inside the microstructure. Both scales are in competition for the localization of cyclic plastic deformation that induces the initiation of the crack that leads to failure.
- When the crack initiates on a defect, it can be of different types: oxide, pore, or shrinkage.
- The critical defect size that does not affect the fatigue limit is 400 μm +/- 100 μm in A356 T6. This result is obtained for both artificial and natural defect and tension, torsion and combined loading for a load ratio R = -1.
- Multiaxial Kitagawa type diagram are simulated using four different approaches: Murakami, LEFM, 'critical distance' and 'gradient'. Results shows that Murakami's equation gives mainly non conservative results for A356-T6 with an average error of 20 % error. LEFM is mainly conservative with an average error of 19 %. Critical distance and gradient are both equivalent with mainly conservative results and average error of respectively 11 and 9 %.

4. REFERENCES:

[1] Murakami Y. Metal fatigue: effects of small defects and non-metallic inclusions. Elsevier; 2002.
[2] Gao YX, Yi JZ, Lee PD, Lindley TC. Acta Mater 2004;52:19.
[3] Brochu M, Verreman Y, Ajersch F, Bouchard D. Int J Fatigue 2010;32:8.
[4] McDowell DL, Gall K, Horstemeyer MF, Fan J. Eng Fract Mech 2003;70:1.
[5] Buffière JY, Savelli S, Jouneau PH, Maire E, Fougères R. Mater Sci Eng A 2001;316:1–2.
[6] Couper MJ, Nesson AE, Griffiths JR. Fatigue Fract Eng Mater Struct 1990;13:3.
[7] Atzori B, Filippi S, Lazzarin P, Berto F. Fatigue Fract Eng Mater Struct 2004;28:1–2.
[8] Dabayeh AA, Xu RX, Du BP, Topper TH. Int J Fatigue 1996;18:2.
[9] Zhu X, Yi JZ, Jones JW, Allison JE. Metall Mater Trans A 2007;38:5.
[10] Kumar A, Torbet CJ, Pollock TM, Jones JW. Acta Mater 2010;58:6.
[11] Vu QH, Halm D, Nadot Y. Int J Fatigue 2010;32:7.
[12] Susmel L, Taylor D. Eng Fract Mech 2008;75:15.
[13] Nadot Y, Billaudeau T. Eng Fract Mech 2006;73:1.
[14] Gadouini H, Nadot Y. Int J Fatigue 2008;30:9.